

Phase Imprinting in Equilibrating Fermi Gases: The Transience of Vortex Rings and Other Defects

Peter Scherpelz,¹ Karmela Padavić,¹ Adam Rançon,¹ Andreas Glatz,^{2,3} Igor S. Aranson,² and K. Levin¹

¹*James Franck Institute and Department of Physics,
University of Chicago, Chicago, Illinois 60637, USA*

²*Materials Science Division, Argonne National Laboratory,
9700 South Cass Avenue, Argonne, Illinois 60439, USA*

³*Department of Physics, Northern Illinois University, DeKalb, Illinois 60115, USA*

(Dated: June 3, 2014)

We present numerical simulations of phase imprinting experiments in ultracold trapped Fermi gases which are in good agreement with recent, independent experimental results. Our focus is on the sequence and evolution of defects using the fermionic time-dependent Ginzburg-Landau equation, which contains dissipation necessary for equilibration. In contrast to other simulations we introduce small, experimentally unavoidable symmetry breaking, particularly that associated with thermal fluctuations and with the phase imprinting tilt angle, and illustrate their dramatic effects. The former causes vortex rings in confined geometries to move to the trap surface and rapidly decay into more stable vortex lines, as appears consistent with recent experimental claims. The latter aligns the precessing and relatively long-lived vortex filaments, rendering them difficult to distinguish from solitons.

Introduction. The evolution of defects (solitons or domain walls, vortices, cosmic strings, monopoles, and other topological structures) is central to many sub-disciplines in physics, including cosmology, as well as condensed matter and fluid dynamics. An issue of broad interest is the way in which the nature of the defects changes as equilibration ensues, reflecting the specifics of the initial perturbation as well as the boundary conditions. In trapped superfluid atomic gases one has access to real time dynamics. Here, rapid cooling from the normal phase [1, 2], sudden density cuts [3] and phase imprinting all have led to a sequence of defects which may, in some cases, be relevant to the Kibble-Zurek mechanism in cosmology as well as to superfluid turbulence.

Phase imprinting is a quite violent alteration of the superfluid in which part of the superfluid experiences a phase shift close to π . This perturbation has attracted recent attention in trapped Fermi gas superfluids because of reports of rather long-lived solitons having anomalously large effective masses and oscillation periods [4]. These dark solitons are planar density depletions which maintain their shape and are associated with phase changes, often close to π . Subsequently, there has been a more in-depth analysis of these experiments [5] which associates these original solitonic observations with long-lived line vortices. These so-called “solitonic” vortices are to be viewed as vortex filaments in an anisotropic trap.

In this paper we present numerical simulations which relate to these phase imprinting experiments. Our work supports the notion of a natural hierarchy towards less extended and less complex defects (soliton to vortex ring to single vortex) during the processes of equilibration. One might similarly expect that the simplest defects are often the most difficult to relax; indeed, we find that

the residual filamentary vortices continue for some time to precess around the atomic cloud. Additionally we find that a very small tilt of the phase imprinting angle is sufficient to consistently align this line vortex in the trapped gas. The picture that emerges is one that appears generally consistent with recent experimental reports [5]. The above observations underline a key contribution of this paper: to show how simulations of defect evolution require one to subject the numerics to checks for robustness against unavoidable broken spatial symmetries in the experiment.

Our work should be contrasted with previous numerical simulations of the Gross-Pitaevskii (GP) and Bogoliubov-de Gennes (BdG) equations which addressed the previously claimed solitonic stability and attributed it instead to vortex rings (that is, vortex lines which are closed into a loop) [6, 7]. These past simulations (omitting noise or other broken symmetries, and in many cases omitting dissipation) do not appear to exhibit all the transitions necessary for the full equilibration of the cloud. Thus the literature [6, 7] has focused on symmetric vortex rings which maintain inversion symmetry about the z -axis [parity transformation (x, y) to $(-x, -y)$] and often apply initial conditions specifically designed to produce a stable vortex ring. In recent work which introduced a small trap anisotropy [7], there were reports of a vortex ring breaking into two vortex lines. However, in this work reflection symmetries were still maintained, so that the two lines of opposite vorticity perpetually move along the longitudinal axis, and after nearing the edge recombine into a ring moving in the opposite direction. We show that these complex processes, which do not bring the system closer to equilibration, are not found here and are overwhelmed by other symmetry breaking features.

Our approach. In contrast to the bosonic GP dy-

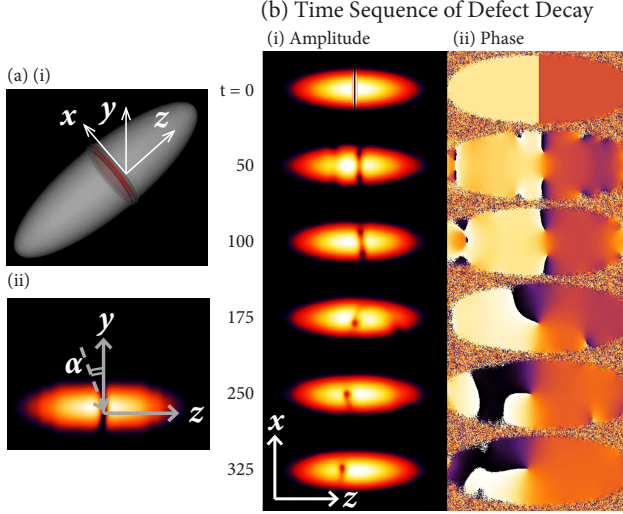


FIG. 1. (Color online) (a) Depictions of axes used. (i) 3D rendering of initial depletion plane (red) with axes used in the paper: y is vertical, and z is the long axis of the trap. (ii) Side view of axes at $t = 20$ after phase imprinting for the run in (b), along with the tilt of the imaging beam, α , considered later in this work. (b) TDGL simulation results for one time sequence, focusing on the vortex ring decay, of a phase imprinting applied at $t = 0$ with $\lambda = 3.3$ and parameters as in the text. (i) shows the cloud density integrated along y and (ii) the phase in the $y = 0$ plane [from 0 (black) to 2π (white)]. Here phase imprinting has formed a ring ($t = 50$), which is just slightly off center. The ring moves toward the cloud edge ($t = 100$), then impacts the edge and decays to a vortex line ($t = 175$).

namics, we use the complex time-dependent Ginzburg-Landau (TDGL) equation [8] for fermionic superfluids, to address three-dimensional (3D) anisotropic trapped Fermi gases subjected to a near- π phase imprinting quench [4]. We consider a harmonic confining potential $V(\mathbf{x}) = (\omega_{\perp}^2(x^2 + y^2) + \omega_z z^2)/2$, where ω_{\perp} and ω_z define how tightly confining the trap is in comparison to the chemical potential, as well as the trap ratio $\lambda = \omega_{\perp}/\omega_z$. Our central TDGL equation is $e^{-i\theta} \partial_t \psi(\mathbf{x}, t) =$

$$\left\{ [1 - V(\mathbf{x})] + \frac{1}{2} \nabla^2 - |\psi(\mathbf{x}, t)|^2 \right\} \psi(\mathbf{x}, t) + \chi(\mathbf{x}, t), \quad (1)$$

where χ is uniformly distributed thermal noise. Equation (1) contains two parameters, in addition to the trap frequencies. First, θ controls the amount of dissipation, effectively moving from BCS ($\theta = 0$, dissipative) to BEC ($\theta = \pi/2$, reducing to the time-dependent GP equation, or equivalently the nonlinear Schrödinger equation). Second, through $\langle \chi(\mathbf{x}, t) \chi^*(\mathbf{x}', t') \rangle = 2\gamma T_{\chi} \delta(\mathbf{x} - \mathbf{x}') \delta(t - t')$, a fluctuation temperature can be set [1, 9–11]. In this work the dimensionless fluctuation temperature is chosen to be very close to the zero-temperature limit, with $\gamma T_{\chi} = 2 \times 10^{-9}$ [1]. Beyond these parameters, the rescaling to this normalized form follows from Ref. [8].

A TDGL approach [12–14] can be viewed as a dissipative GP simulation where the dissipation becomes progressively stronger as the dynamics changes from propagating (in BEC) to diffusive (in BCS), reflecting the fact that pairs are in equilibrium with the underlying fermions. Along with this dissipation is a stochastic contribution required to simulate finite temperatures or experimental imperfections [1]. Higher levels of microscopic self consistency lead to longer-lived pairs in the intermediate (near-unitary) regime [13, 14], as compared to earlier estimates of the TDGL coefficients. This effectively reduces the dissipation (increases θ). We use $\theta = 88^\circ$ for simulations here, with the amount of dissipation primarily affecting the lifetime of the resulting vortex line described below. [See Supplementary materials (SI) for more details.]

Our studies are based on numerical simulations discretized in 512^3 grid points designed to solve Equation (1) using a quasi-spectral split-step method. The simulations are performed on a GPU computing cluster, allowing relatively large simulation sizes. The initial condition is found using a heat diffusion equation to cool the system to equilibrium before the phase imprinting is applied, as in Ref. [1]. Within this TDGL approach for Fermi gases, the form and rescaling of the trap potential is inserted via the local density approximation, $\mu \rightarrow \mu - V(\mathbf{x})$, where μ is the chemical potential [normalized to 1 in Eq. (1)]. In the bosonic TDGL limit, this trap potential form is identical to that used in GP [15], and away from this limit, it is slightly rescaled.

Our detailed findings: Transience of defects. We investigated a system with axial (xy) symmetry, $\omega_z = 0.038\mu/\hbar$, and a variable trap ratio $\lambda = \omega_{\perp}/\omega_z$. The parameters used here match the trap ratios and symmetries in Ref. [4], but with a somewhat larger ω/μ which provides more fine-grained computational resolution of the defects. We will focus on the case $\lambda = 3.3$. In more anisotropic traps with $\lambda = 6.2$, we find the vortex ring is even more transient, immediately colliding with the cloud edge to leave a line vortex. Finally, in quasi-1D clouds with $\lambda = 15.0$, the system cannot nucleate vortices and a reasonably stable soliton appears which oscillates along the axial direction of the trap, in agreement with 1D predictions.

After the cloud has reached equilibrium, we imprint a 175° phase shift in the middle of the cloud [in a plane perpendicular to z , with axes shown in Fig. 1(a)], and observe the evolution. Images from a typical run are displayed in Figure 1(b) (see also SI). Immediately after the imprint, a planar density depletion forms [first frame in Fig. 1(b)]. However, the plane rapidly deforms along the axial direction (see SI), and a vortex ring forms. This initial formation of the vortex ring through the snake instability [7, 16–20] appears in the second frame of Figure 1(b) [21]. In the absence of noise and dissipation, this ring is stable and oscillates in the trap, as observed in

other simulations [6, 7]. The presence of noise perturbs part of the ring, moving it closer to the boundary. The third and fourth frames illustrate the ring collision with the boundary.

The observed tilting and attraction of the vortex ring to the boundary can be qualitatively understood by applying the method of images [22] to vortex dynamics. (See SI for more details.) By considering the simplified case of the ring's interaction with a hard planar boundary, an image vortex ring can be introduced to satisfy the boundary conditions [22]. This approximation still captures the main dynamics of the trapped vortex ring [23, 24]. In this approximation the ring propagates along the boundary due to advection by supercurrents, but the image vortex retards that part nearest the boundary leading to a tilt [25, 26]. Finally, the tilted ring is attracted to the boundary, and “reconnects” with the image ring, resulting in a vortex line attached to the boundary [see Figure 1(b)]. The reconnection dynamics are essentially the same as that of the reconnection between two vortex lines [22, 27, 28].

The stability of these line and ring defects, and their robustness to unavoidable noise and broken symmetries, are critical to properly compare simulations to experiment. In Figure 2(a) we plot the defect lifetime as a function of the initial phase imprinting angle applied. The vortex ring always decays relatively rapidly, through shrinking to zero radius at small imprinting angles or from impacting the trap edge at larger angles. However, at the large phase imprinting angles appropriate to experiment, the vortex line that remains after ring decay can persist for a relatively long time, as in Figure 2(b-c), where multiple cycles of the vortex line precession are observed. These lifetimes are controlled by the advection of the defects, which in turn depends on both the local phase gradient and the superfluid density depletion. Similar to solitonic behavior [29], small phase shifts lead to large defect velocities, while phase shifts close to π cause large density depletions and apply very little momentum to the defects. These low velocities significantly contribute to the long vortex lifetime in this regime [30].

A more detailed view of this precessing trajectory is shown in Figure 2(b). At the earliest times, when the vortex is near the cloud center, it has a smaller-scale rotation in the counterclockwise direction in addition to the main precession of the vortex in the clockwise direction. This smaller-scale rotation, seemingly due to the decay of the other portion of the ring, gradually subsides, and the remaining precession and outward movement of the vortex are typical in the presence of dissipation (see also SI) [26, 31]. The precession of this line vortex could appear as a traveling density depletion. This is illustrated in Figure 2(c), under the assumption that the vortex line was precessing in a plane that is nearly orthogonal to the one observed.

Comparison to Experiment. The results and interpre-

tations of recent experiments [5] agree well with the vortex line observations described above. What remains to be understood, then, is what determines the line vortex orientation. As demonstrated by the results of multiple runs in Figure 2(d.i), without further symmetry breaking, our simulations produce vortex lines with random orientations. (Similarly, note that the run used in Figs. 1(b) and 2(b-c) has a random vortex orientation which does not match experiment.) In order for the lines to have robust alignment, as has been found in the most recent experimental analysis [5], other symmetry-breaking features must be present. One proposed possibility is that asymmetries in the perpendicular trap frequencies ω_x and ω_y govern the vortex orientation [5]. Another alternative is a slightly tilted phase-imprinting beam. With the inclusion of noise in our simulations, we have found that small trap anisotropies, as are reported experimentally [5], do not produce reliable vortex orientations in contrast to recent claims [32]. (It should be noted that in our earlier simulations we were inclined to believe in this mechanism as well, but have since rejected it.) The lack of consistency we find reflects the possibility of reconnection between the two vortices that form, and the relatively chaotic vortex behavior that follows (see SI for details). This is in contrast to the simulations [7, 32] which maintain a reflection symmetry about the yz plane ($x \rightarrow -x$), thus leading to vortex alignments which do not otherwise seem to be stable [33].

A more satisfactory alternative is to include the effects of very small tilts in the phase-imprinting beam, so that it is offset from the vertical axis by an angle α [see Fig. 1(a.ii)] and no longer perpendicular to the long z axis, while remaining perpendicular to the x axis. We find this can reliably determine the vortex orientation, and agrees with the orientation observed in experiment. As this imaging beam cannot be placed perfectly, we believe this is a plausible mechanism for determining the orientation of the vortex line. This is shown in Figure 2(d.ii). As noted in Ref. [5], slight tilts of the initial planar depletion can lead to different effects. Here, we find that for tilts in the imprinting beam of $\alpha = 1^\circ$ or smaller, a vortex ring is produced which quickly decays to a vortex line, as in the absence of this symmetry breaking. The degree of tilt needed to orient the line is dependent on the magnitude of the noise introduced. For typical values of our small noise prefactor, an $\alpha \approx 0.05^\circ$ tilt is adequate. Furthermore, for a 1° tilt we find that moderate anisotropies have no discernible influence upon the ultimate orientation of the vortex line, though it may add an additional decay step (see SI).

Thus far, our simulations (with these small broken symmetries) lead us to believe that what was observed experimentally [4] was not a long-lived soliton but rather this residual precessing vortex filament which can be imaged as in Figure 2(c). However, in order to fully compare with experiments, one needs to address the period

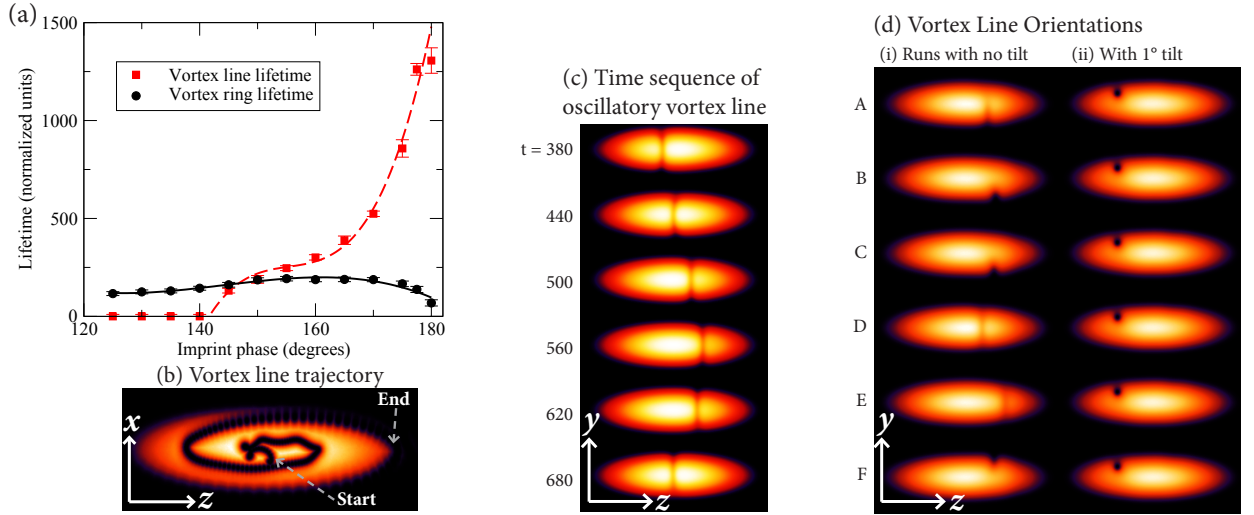


FIG. 2. (Color online) (a) Lifetimes of defects as a function of the imprinting phase, using the same parameters as in Figure 1(b). Red squares indicate lifetimes of vortex lines, which are substantially longer than those of vortex rings (black circles). Error bars reflect run-to-run variations and limitations on time estimates. Lines are cubic polynomial fits provided as a guide to the eye. (b) Plots of the trajectory of the precessing single vortex near the end-stage of equilibration for the same run. Here frames (cuts of $|\psi|^2$ along the $y = 0$ plane) with $\Delta t = 5$ were combined and the minimum density among all frames selected, displaying the vortex trajectory during $t = [180, 1160]$. (c) A series of density plots for the $\lambda = 3.3$ run in Figure 1(b), integrated along the x axis, during the interval in which only one vortex is present. The density effectively shows a line depletion due to the orientation of the vortex, which oscillates along the cloud. (d) Comparison of a (d.i) perfectly orthogonal phase imprinting and (d.ii) phase imprinting with a beam tilted by 1° relative to the vertical axis, leaving it orthogonal to the x (short horizontal) axis but not to the z (loosely confined horizontal) axis. Each cell is integrated along x at $t = 400$ for a run with different random noise, but conditions otherwise unchanged. This shows that without a tilt the vortex can be oriented many different directions (d.i), but a small tilt stabilizes the orientation in different runs (d.ii).

of oscillations and the associated trends from the BCS to BEC sides of unitarity. In general, we expect that for constant trap parameters, the period of the precession of a vortex line will follow the size of the superfluid cloud. This means that as the system approaches unitarity from the BEC side, the increase in interaction strength will expand the cloud and lead to a longer precession period. Similarly, if ω_\perp is kept constant and λ decreased, the weaker z -axis confinement will increase the cloud size and lead to a longer precession period. Both of these trends match the BCS-BEC variation observed experimentally [4]. These predictions can be quantified using the Thomas-Fermi (TF) approximation. In this case the precession frequency has been derived as [34–36]

$$\omega_p = \frac{3\hbar\omega_z\omega_\perp}{M(\omega_z^2 + \omega_\perp^2)R_{xz}^2} \log\left(\frac{R_{xz}}{\xi}\right) \frac{1}{1 - r_0^2}, \quad (2)$$

where ξ is the healing length, $R_{xz}^2 = 4\mu/[M(\omega_z^2 + \omega_\perp^2)]$ defines an effective trap radius, and $r_0 = (x/R_x, z/R_z)$ is the dimensionless vortex position. Using the TF approximation [15] for the parameters μ and ω_\perp given in Ref. [4] at unitarity, we obtain a very rough estimate of the ratio of the vortex period to the trap period as $T_v/T_z = 10.2/(1 - r_0^2)$, in reasonable agreement with the reported results near unitarity. Our simulations also agree with Equation (2) (see SI).

Conclusion. These simulations strongly support the conclusion that earlier experimental observations [4], interpreted as stable solitons, were in fact precessing vortex lines. We note that this simulation-based attribution of the experimental observations to vortex lines preceded more recent experiments [5]. Adding to the support for our physical picture is the fact that the oscillation period associated with the precessing vortex filament [Eq. (2)] depends directly on the cloud size squared, and that this period will be longest in the BCS and shortest in the BEC regimes. Finally, important is the rather robust vortex line alignment we find with a very small tilt of the phase imprinting angle.

This work demonstrates that in future simulations of superfluid dynamics, the stability of the results should be demonstrated when imperfections (whether thermal fluctuations, small anisotropies, misalignments, etc.) are included. These processes can be necessary for simulations to mimic real-world experiments, and to properly model the dynamics which lead to ultimate equilibration.

This work is supported by NSF-MRSEC Grant 0820054. Work at Argonne was supported by the Scientific Discovery through Advanced Computing (SciDAC) program funded by U.S. Department of Energy, Office of Science, Advanced Scientific Computing Research (large-scale GPU simulations) and Basic Energy Sciences, and

by the Office of Science, Materials Sciences and Engineering Division (modeling/analysis). The numerical work was performed on NIU's GPU cluster GAFA. P.S. acknowledges support from the Hertz Foundation. Finally, we are grateful to William Irvine, Ariel Sommer and Michael Forbes for insightful discussions.

-
- [1] A. Glatz, H. L. L. Roberts, I. S. Aranson, and K. Levin, *Phys. Rev. B* **84**, 180501 (2011).
 - [2] C. N. Weiler, T. W. Neely, D. R. Scherer, A. S. Bradley, M. J. Davis, and B. P. Anderson, *Nature* **455**, 948 (2008).
 - [3] M. R. Andrews, D. M. Kurn, H.-J. Miesner, D. S. Durfee, C. G. Townsend, S. Inouye, and W. Ketterle, *Phys. Rev. Lett.* **79**, 553 (1997).
 - [4] T. Yefsah, A. T. Sommer, M. J. H. Ku, L. W. Cheuk, W. Ji, W. S. Bakr, and M. W. Zwierlein, *Nature* **499**, 426 (2013).
 - [5] M. J. H. Ku, W. Ji, B. Mukherjee, E. Guardado-Sanchez, L. W. Cheuk, T. Yefsah, and M. W. Zwierlein, arXiv:1402.7052 [cond-mat.quant-gas] (2014).
 - [6] A. Bulgac, M. M. Forbes, M. M. Kelley, K. J. Roche, and G. Wlazlowski, *Phys. Rev. Lett.* **112**, 025301 (2014).
 - [7] M. D. Reichl and E. J. Mueller, *Phys. Rev. A* **88**, 053626 (2013).
 - [8] I. S. Aranson and L. Kramer, *Rev. Mod. Phys.* **74**, 99 (2002).
 - [9] I. S. Aranson, N. B. Kopnin, and V. M. Vinokur, *Phys. Rev. Lett.* **83**, 2600 (1999).
 - [10] B. Damski and W. H. Zurek, *Phys. Rev. Lett.* **104**, 160404 (2010).
 - [11] A. Schmid, *Phys. Rev.* **180**, 527 (1969).
 - [12] C. A. R. Sá de Melo, M. Randeria, and J. R. Engelbrecht, *Phys. Rev. Lett.* **71**, 3202 (1993).
 - [13] J. Maly, B. Jankó, and K. Levin, *Physica C: Superconductivity* **321**, 113 (1999).
 - [14] J. Maly, *Pseudogap effects in a precursor superconductivity model of the cuprates*, Ph.D. thesis, The University of Chicago, United States – Illinois (1997).
 - [15] C. Pethick and H. Smith, *Bose-Einstein Condensation in Dilute Gases*, 2nd ed. (Cambridge University Press, Cambridge, 2008).
 - [16] C. A. Jones, S. J. Putterman, and P. H. Roberts, *J. Phys. A* **19**, 2991 (1986).
 - [17] A. V. Mamaev, M. Saffman, and A. A. Zozulya, *Phys. Rev. Lett.* **76**, 2262 (1996).
 - [18] A. V. Mamaev, M. Saffman, D. Z. Anderson, and A. A. Zozulya, *Phys. Rev. A* **54**, 870 (1996).
 - [19] V. Tikhonenko, J. Christou, B. Luther-Davies, and Y. S. Kivshar, *Opt. Lett.* **21**, 1129 (1996).
 - [20] D. L. Feder, M. S. Pindzola, L. A. Collins, B. I. Schneider, and C. W. Clark, *Phys. Rev. A* **62**, 053606 (2000).
 - [21] Sound waves are also produced by phase imprinting, but dissipate as they reach the trap edge, a key benefit of the dissipation included in these simulations. This agrees with experimental observations [4] and is in contrast to the behavior of sound modes in GP simulations [6, 7].
 - [22] K. W. Schwarz, *Phys. Rev. B* **31**, 5782 (1985).
 - [23] P. Mason and N. G. Berloff, *Phys. Rev. A* **77**, 032107 (2008).
 - [24] P. Mason, N. G. Berloff, and A. L. Fetter, *Phys. Rev. A* **74**, 043611 (2006).
 - [25] J. R. Anglin, *Phys. Rev. A* **65**, 063611 (2002).
 - [26] N. G. Parker, B. Jackson, A. M. Martin, and C. S. Adams, in *Emergent Nonlinear Phenomena in Bose-Einstein Condensates*, Atomic, Optical, and Plasma Physics No. 45, edited by P. P. G. Kevrekidis, P. D. J. Frantzeskakis, and P. R. Carretero-González (Springer Berlin Heidelberg, 2008) pp. 173–189.
 - [27] E. D. Siggia, *Phys. Fluids* **28**, 794 (1985).
 - [28] J. Koplik and H. Levine, *Phys. Rev. Lett.* **71**, 1375 (1993).
 - [29] T. Busch and J. R. Anglin, *Phys. Rev. Lett.* **84**, 2298 (2000).
 - [30] This phase-dependence on vortex line velocity reflects the behavior of “solitonic vortices” described in recent experiments [5, 37]. In all of these cases, the “solitonic vortex” is simply the vortex line with dynamics influenced by the inhomogeneous, elongated trap it is placed in. Note that this is in contrast to early discussions of solitonic vortices [38–40], which focus on quasi-1D systems which are dissimilar to these recent experiments and simulations.
 - [31] B. Jackson, J. F. McCann, and C. S. Adams, *Phys. Rev. A* **61**, 013604 (1999).
 - [32] G. Wlazlowski, A. Bulgac, M. M. Forbes, and K. J. Roche, arXiv:1404.1038 [cond-mat.quant-gas] (2014).
 - [33] Other recent simulations in BECs [41] showed the expected vortex orientation due to anisotropy, but only with very large anisotropy $\omega_y/\omega_x \sim 1.6$.
 - [34] A. L. Fetter and J.-k. Kim, *J. Low Temp. Phys.* **125**, 239 (2001).
 - [35] A. A. Svidzinsky and A. L. Fetter, *Phys. Rev. Lett.* **84**, 5919 (2000).
 - [36] A. L. Fetter and A. A. Svidzinsky, *J. Phys. Condens. Matter* **13**, R135 (2001).
 - [37] S. Donadello, S. Serafini, M. Tylutki, L. P. Pitaevskii, F. Dalfovo, G. Lamporesi, and G. Ferrari, arXiv:1404.4237 [cond-mat.quant-gas] (2014).
 - [38] J. Brand and W. P. Reinhardt, *J. Phys. B* **34**, L113 (2001).
 - [39] J. Brand and W. P. Reinhardt, *Phys. Rev. A* **65**, 043612 (2002).
 - [40] N. Parker, *Numerical Studies of Vortices and Dark Solitons in Atomic Bose-Einstein Condensates*, Ph.D. thesis, Durham University (2004).
 - [41] C. Becker, K. Sengstock, P. Schmelcher, P. G. Kevrekidis, and R. Carretero-Gonzalez, *New J. Phys.* **15**, 113028 (2013).

SUPPLEMENTARY MATERIAL

Detailed Decay of the Defect

A 3D visualization of the main simulation run analyzed in the text is shown in Fig. S1. Sound waves are produced and dissipate at $t = 8$ through $t = 80$. At the same time, the inner core of the planar density depletion “bows out” at $t = 24$, leading to the depletion transforming into a vortex ring ($t = 48$) as fluid returns to the middle of the superfluid. Past this point, the decay of the vortex ring, for example $t = 144$, and the precession of the resulting vortex line from $t = 176$ to $t = 700$ can be observed.

Method of Images

To qualitatively describe the decay of the vortex ring presented in the main paper, we use the method of images by considering the interactions of a hard boundary which is approximated as a plane. This approach can give an intuitive picture for the movement of the vortex ring and vortex line, and it also draws on techniques shared with electromagnetism. Although this approach is qualitative [1–3] it can provide valuable insight into vortex behavior near boundaries [4]. Importantly, these image ring arguments match our observations in the above simulations.

In more detail, to use the method of images with a hard boundary, one begins with the condition that the normal component of the superfluid velocity is zero on the boundary, $\mathbf{v}_s \cdot \mathbf{n} = 0$. In direct analogy with the magnetic field generated by current flowing through a wire, the velocity fields created by vortices in the absence of boundaries follows the Biot-Savart law [5]:

$$\mathbf{v}_{s,w}(\mathbf{r}) \equiv \frac{\kappa}{4\pi} \int_{\mathcal{L}} \frac{(\mathbf{s} - \mathbf{r}) \times d\mathbf{s}}{|\mathbf{s} - \mathbf{r}|^3} + \mathbf{v}_{s,i}, \quad (1)$$

where the integral goes over the vortex line(s), κ is the quantized vortex circulation, and $\mathbf{v}_{s,i}$ is due to imprinting. However, to satisfy the boundary condition $\mathbf{v}_s \cdot \mathbf{n} = 0$, a second (boundary) velocity field $\mathbf{v}_{s,b}$ is added, with $\nabla \cdot \mathbf{v}_{s,b} = 0$ and $\nabla \times \mathbf{v}_{s,b} = 0$, such that

$$(\mathbf{v}_{s,w} + \mathbf{v}_{s,b}) \cdot \mathbf{n} = 0. \quad (2)$$

For a plane boundary, $\mathbf{v}_{s,b}$ is the field created by an image vortex, which is the real vortex reflected along the boundary with the vortex direction reversed [5].

A diagram of this image vortex behavior is presented in Figure S2. As can be seen in this figure, and as described in the main text and seen in simulations, the boundary has two major effects. First, it retards the movement of the portion of the vortex ring nearest the boundary, resulting in a tilt of the ring as a whole. Second, because vortices of opposite direction attract each other, the ring is attracted to its image, and eventually reconnects with it. Thus, the use of images, controlled by application of boundary conditions and the Biot-Savart law, leads directly to a qualitative description of the ring decay observed in these simulations.

Vortex Decay in Anisotropic Traps

Recent experimental work [6] has postulated that the reliable vortex orientations produced are due to a slight difference in the trapping frequencies ω_x and ω_y , primarily due to the force of gravity decreasing the effective ω_y . In this trap configuration, the vortex is in its lowest energy state if oriented parallel to the x axis, which would agree with experiment. However, recent work [7] has pointed out that the relaxation of the vortex line to this orientation may be quite slow. While Ref. [7] shows other potential mechanisms that result in this vortex decay, as we note in the main text, their simulations depend on maintaining a reflection symmetry.

In contrast to these suggestions, we find that the vortex orientation in an anisotropic trap can be very sensitive both to the details of the experimental configuration, as well as to random perturbations of the system. Some of these features are explored in Figure S3(A-C). More specifically, Fig. S3(A) shows a large system in which the ring impacts both sides of the trap, and breaks apart into two vortices. However, after a period of time these two vortices reconnect, a fairly chaotic process that rapidly ejects one vortex line, leaving a single vortex line in the trap. This remaining vortex line can have a fair degree of freedom in its orientation, as shown in $t = 850$ for (A). In Fig. S3(B), the ring similarly splits into two vortices, but these vortices move far enough apart that they do not reconnect, similar

to the case for large anisotropies reported in Ref. [9]. This produces the desired vortex orientation, but we do not observe it occurring reliably. Fig. S3(C) is similar to (A), but for a smaller system, and is a very common decay mechanism that we observe in anisotropic traps, with a relatively free final vortex orientation.

When a tilt is applied in the presence of an anisotropic trap, we find that the tilt appears to determine the vortex orientation. In Fig. S3(D) a 1° tilt is applied perpendicular to the x axis. The vortex ring does break apart into two vortex lines, but these two vortex lines reliably avoid reconnection, with one of the two quickly leaving the trap. We note that this tilt of the beam seems reasonable given the fact that the phase imprinting beam is sent from above the cloud [10], so it could be slightly tilted away from parallel to the y -axis, while still applying a nearly symmetric cut of the cloud along the x direction.

In contrast, in Fig. S3(E) the tilt is applied perpendicular to the y axis (opposite what might be seen in experiment), and the final vortex orientation follows the tilt rather than the trap anisotropy. Specifically, in (E) the initial vortex ring quickly collides with one edge of the trap, leaving a vertically oriented vortex line.

In summary, we find that some mechanisms of vortex ring decay in an anisotropic trap do reproduce the vortex orientation seen experimentally [6]. However, when noise is included, we do not find that these orientations are robust. Instead, if a tilt in the imprinting beam is present, the tilt robustly dictates the vortex line orientation.

Periods and Dissipation

The periods which we measure for our simulations seem to agree well with theoretical predictions. For our simulations (with smaller μ/ω_\perp values compared to the experiments), Eq. (2) of the manuscript predicts $T_v/T_z = \{3.5, 2.3\}(1 - r_0^2)$ for $\lambda = \{3.3, 6.2\}$ respectively (with T_v the vortex line period, and $T_z = 2\pi/\omega_z$). We measured an average $T_v/T_z = \{2.4 \pm 0.3, 1.6 \pm 0.2\}$ for these λ , which agree for $r_0 \approx 0.7$. We also observed the predicted decrease in period as the vortex moves to larger radii. Furthermore, although the vortex ring exhibited the slowest oscillation of the defects considered (we reduced noise to 0 and observed $T_{vr}/T_z = 1.8 \pm 0.2$ for $\lambda = 6.2$), the distinction between it and the line vortex is not large, and we do not consider the oscillatory period found in the experiment to point to definitive proof of a vortex ring [11]. Finally, for the quasi-1D case with $\lambda = 15$, we measure the soliton period T_s as $T_s/T_z = 1.39 \pm 0.03$, in good agreement with the predicted $T_s/T_z = \sqrt{2}$ value for solitons in the GP system.

Figure S4 shows the effect of changing the dissipation angle θ in these simulations. At small angles, the high dissipation causes the vortex line to very quickly leave the superfluid. In contrast, at large angles, where dissipation is very small, the vortex can precess for many cycles around the cloud, and moves toward the edge very slowly. This is in agreement with the theoretical expectations for the effect of dissipation [12].

Also available are movies [13] which show integrated cloud densities at $\theta = 86^\circ$, 88° , and 89.5° . In the movie with 89.5° , two effects of low dissipation can be seen: Non-topological density fluctuations (i.e. sound waves) persist for a long period of time, and the vortex precesses for many cycles before dissipating at the trap edge.

-
- [1] P. Mason and N. G. Berloff, Phys. Rev. A **77**, 032107 (2008).
 - [2] P. Mason, N. G. Berloff, and A. L. Fetter, Phys. Rev. A **74**, 043611 (2006).
 - [3] J. R. Anglin, Phys. Rev. A **65**, 063611 (2002).
 - [4] While Ref. [3] argues against the use of image vortices for quantitative work in trapped gases, the author does acknowledge their qualitative predictions are usually accurate. Furthermore, Ref. [1] is able to use image vortices to analyze essentially the same problem.
 - [5] K. W. Schwarz, Phys. Rev. B **31**, 5782 (1985).
 - [6] M. J. H. Ku, W. Ji, B. Mukherjee, E. Guardado-Sanchez, L. W. Cheuk, T. Yefsah, and M. W. Zwierlein, arXiv:1402.7052 [cond-mat.quant-gas] (2014).
 - [7] G. Wlazlowski, A. Bulgac, M. M. Forbes, and K. J. Roche, arXiv:1404.1038 [cond-mat.quant-gas] (2014).
 - [8] T. Yefsah, A. T. Sommer, M. J. H. Ku, L. W. Cheuk, W. Ji, W. S. Bakr, and M. W. Zwierlein, Nature **499**, 426 (2013).
 - [9] C. Becker, K. Sengstock, P. Schmelcher, P. G. Kevrekidis, and R. Carretero-Gonzalez, New J. Phys. **15**, 113028 (2013).
 - [10] A. Sommer, Private communication (2014).
 - [11] Note that for this run, double precision was used but with a smaller computational grid of edge size $L = 256$ rather than $L = 512$ used in the rest of the paper.
 - [12] N. G. Parker, B. Jackson, A. M. Martin, and C. S. Adams, in *Emergent Nonlinear Phenomena in Bose-Einstein Condensates*, Atomic, Optical, and Plasma Physics No. 45, edited by P. P. G. Kevrekidis, P. D. J. Frantzeskakis, and P. R. Carretero-González (Springer Berlin Heidelberg, 2008) pp. 173–189.
 - [13] Available at <http://mti.msd.anl.gov/highlights/coldfermions>.

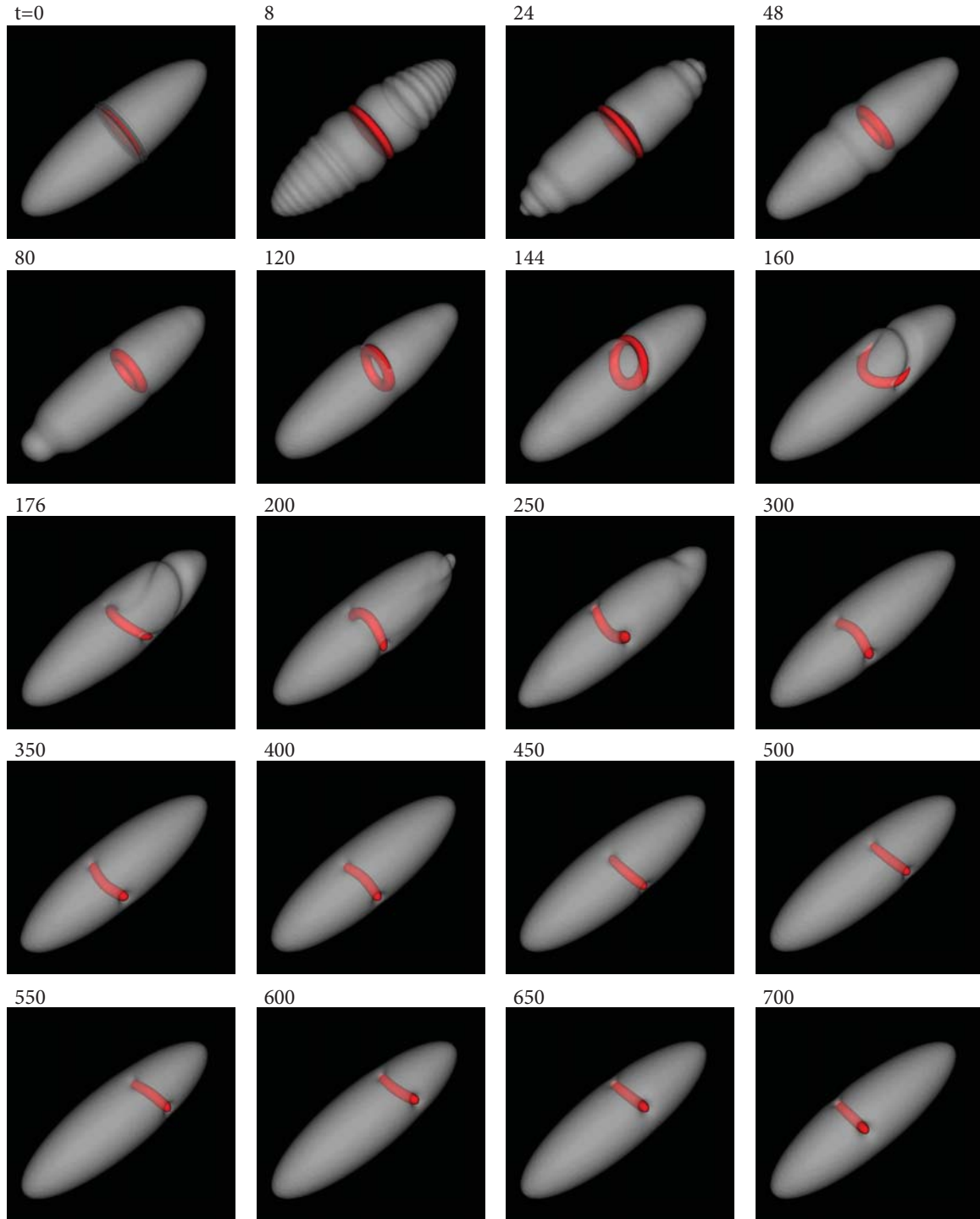


FIG. 1. A time sequence of 3D images for the run in Figure 1(b) at the indicated times. Each timestep includes an isosurface of $|\psi|^2$ (white) and of $|\psi_e|^2 - |\psi|^2$ (red). Here $|\psi_e|^2$ is the superfluid amplitude measured just prior to the phase cut, when the cloud is in equilibrium.

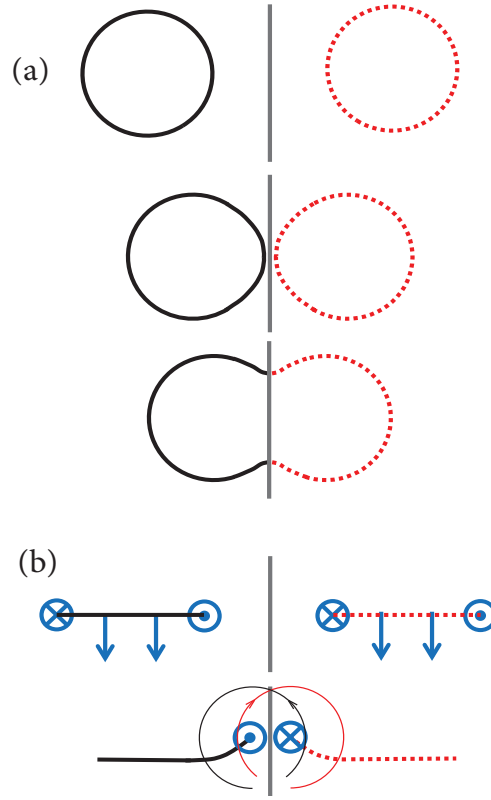


FIG. 2. Illustration of a vortex ring (black) to image ring (dotted red) reconnection process [5], from top to bottom and viewed along the z axis in (a). Panel (b) shows the side view parallel to the boundary plane and vortex ring plane. Circulation corresponds to $\{\odot, \otimes\}$ for counterclockwise and clockwise rotation, respectively, in this view. Arrows indicate velocities induced by the vortex ring segments nearest the surface.

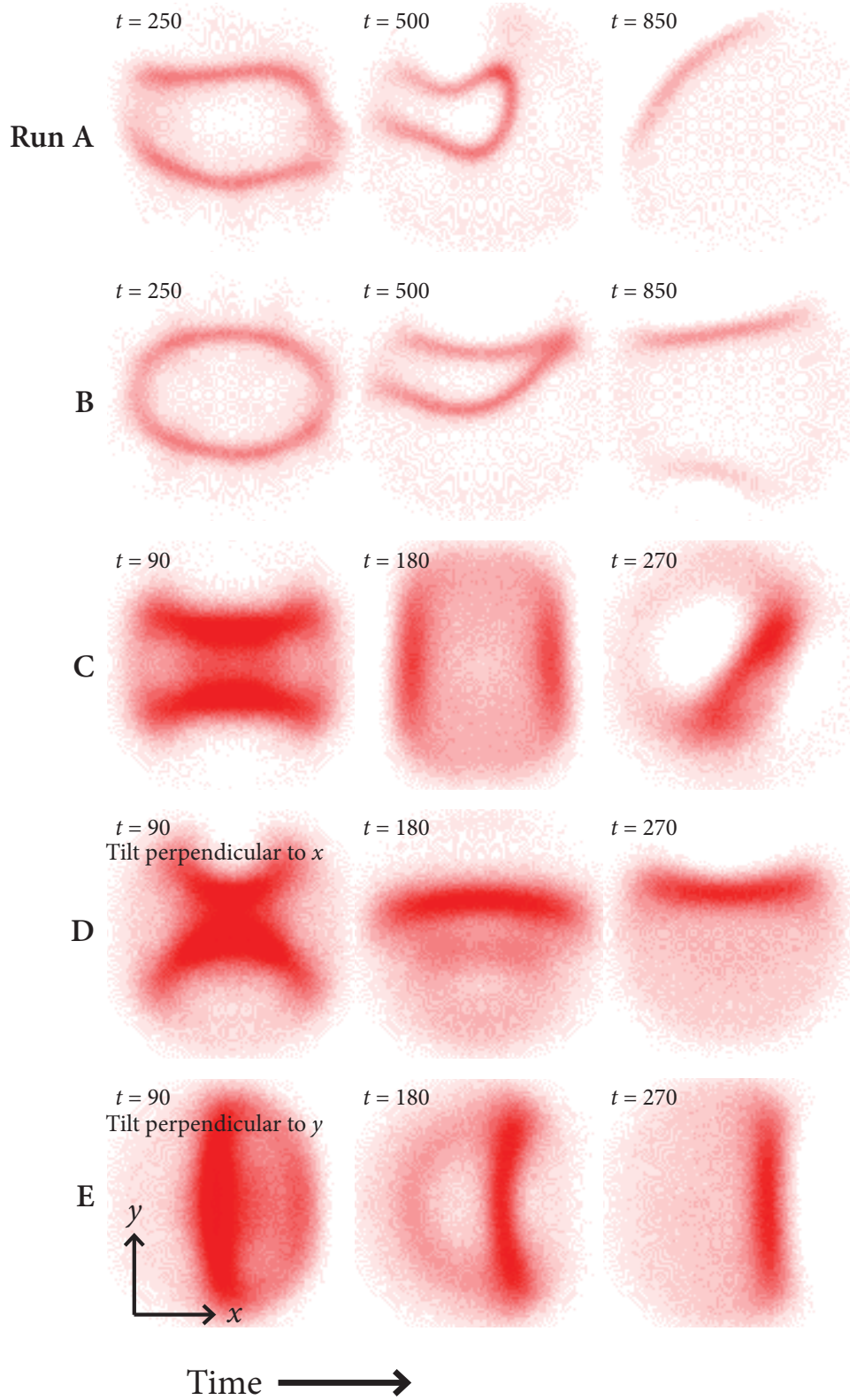


FIG. 3. Results of simulations runs in anisotropic traps. Each row shows a time sequence of vortex evolution in one simulation run. Displayed are residuals of the cloud density, integrated along the z (long horizontal) axis. The red color represents regions of the integrated cloud which are less dense than the density for the equilibrated cloud. All clouds here have $\omega_y < \omega_x$, with $\omega_y/\omega_x \approx 0.96$, which reflects both the direction and magnitude of anisotropy reported in recent experiments [6]. In these figures, the experimentally reported vortex lines [6, 8] would appear as horizontal red lines. Here (A-C) are runs with no tilt of the imaging beam applied, while (D) and (E) do have a tilt applied, as given in the figure. In (A) and (B) all trap frequencies have been reduced by a factor of two to give a larger system size, and the effective temperature for the noise, T_χ , has been decreased by a factor of about 12 compared to all other runs in this manuscript.

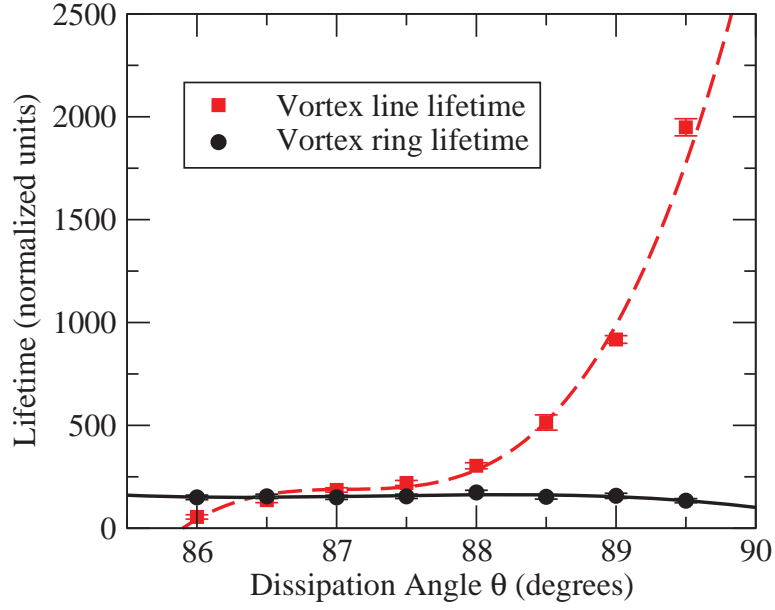


FIG. 4. The lifetime of defects as a function of the dissipation angle θ used in the simulations. The vortex ring lifetime (black circles) is relatively consistent with the angle, while large values of θ give very large vortex line lifetimes (red squares). Lines are cubic polynomial fits provided as a guide to the eye. Note that rather than a step function phase imprinting, these simulations used a phase imprinting formula of $\Delta\phi = \frac{1}{2} [1 + \tanh(-x/\delta)]$ with $\delta = 0.1$ in normalized units. This causes lifetimes here to differ somewhat compared to Fig. 2(a) of the manuscript